Int. J. Electrochem. Sci., 6 **(2011)** 5649 - 5675

International Journal of
ELECTROCHEMICAL
SCIENCE
www.electrochemsci.org

Computational Simulation and Statistical Analysis on the Relationship Between Corrosion Inhibition Efficiency and Molecular Structure of Some Phenanthroline Derivatives on Mild Steel Surface

N.O. Obi-Egbedi[1], *I.B. Obot*[1,2,*], *M.I. El-Khaiary*[3], *S.A. Umoren*[2] *and E.E. Ebenso*[4]

[1] Department of Chemistry, University of Ibadan, Ibadan, Nigeria.
[2] Department of Chemistry, Faculty of Science, University of Uyo, P.M.B 1017, Uyo, Nigeria.
[3] Chemical Engineering Department, Faculty of Engineering, Alexandria University, El-Hadara, Alexandria 21544, Egypt
[4] Department of Chemistry, School of Mathematical & Physical Sciences, North-West University (Mafikeng Campus), Private Bag X2046, Mmabatho 2735, South Africa.
[*]E-mail: proffoime@yahoo.com

Received: 2 September 2011 / *Accepted:* 8 October 2011 / *Published:* 1 November 2011

The density functional theory (DFT) at the B3LYP/631G (d) basis set level was performed on three phenanthroline derivatives used as corrosion inhibitors, namely 2-mesityl-1H-imidazo[4,5-f][1,10]phenanthroline (G), 2-(6-methylpyridin-2-yl)-1H-imidazo[4,5-f][1,10]phenanthroline (J) and 2-(pyridine-2-yl)-1H-imidazo[4,5-f][1,10]phenanthroline (K) to investigate the correlation between molecular structure and the corresponding inhibition efficiency (*I%*). The quantum chemical properties most relevant to their potential action as corrosion inhibitors have been calculated in the neutral and protonated forms in aqueous phase for comparison. Results obtained in this study indicate that indeed, in acidic media, one should consider the protonated species involved because they seem to represent better the actual experimental situation.

Keywords: Phenanthroline derivatives, statistical analysis, mild steel, corrosion inhibitors, sulphuric acid, density functional theory (DFT).

1. INTRODUCTION

The use of acid solution during pickling and industrial cleaning leads to corrosive attack on mild steel. The corrosion of mild steel is of fundamental academic and industrial concern that has received a considerable amount of attention. Among efficient corrosion inhibitors use to prevent the deterioration of mild steel are heterocyclic organic compounds consisting of a π-system and/or O, N, or

S heteroatoms [1-10]. It is generally accepted that organic molecules inhibit corrosion by adsorption on metal surface. Furthermore, the adsorption depends on the electronic structure of inhibiting molecules, steric factor, aromaticity and electron density at donor site, presence of functional groups such as –C=O, -N=N, R-OH, etc., molecular area, molecular weight of the molecule, temperature and electrochemical potential at the metal/solution interface [11-18].

Experimental means are useful in explaining the corrosion inhibition mechanism but they are often expensive and time consuming since it is always based on large scale trial-and error experiments. However, ongoing computer hardware and software advances have opened the door for powerful use of theoretical chemistry in corrosion inhibition research [19]. Quantum chemical calculations can complement the experimental investigations or even predict with confidence some experimentally unknown properties. Recently, there has been increasing use of the density functional theory (DFT) methods as a theoretical tool in elucidating the mechanism of corrosion inhibition of organic compounds by several researchers [20-22]. The advancement in methodology and implementations has reached a point where predicted properties of reasonable accuracy can be obtained from DFT calculations [23]. However, despite enormous literature available on the use of DFT in understanding the corrosion inhibition mechanism, information on the use of statistical analysis as a tool in correlating the experimentally determined inhibition efficiencies and the calculated quantum chemical parameters in the neutral and protonated forms is scare.

This present paper reports the correlation between observed inhibition efficiency of some phenanthroline derivatives used as corrosion inhibitors with their calculated quantum chemical parameters both in the neutral and in the protonated forms using statistical tool. The calculations of global reactivity indices of the inhibitors such as the localization of frontier molecular orbitals, E_{HOMO}, E_{LUMO}, energy gap (ΔE), dipole moment (D), hardness (η), softness (σ), the fractions of electrons transferred (ΔN), electrophilicity index (ω), total energy change (ΔE_T) and Mulliken charge distributions together with local reactivity by means of Fukui indices using DFT at B3LYP/631G (d) basis set level were used to explain the electron transfer mechanism between the inhibitor molecules and the steel surface. Furthermore, statistical equations were proposed using the multiple-linear and the non-linear regression analysis.

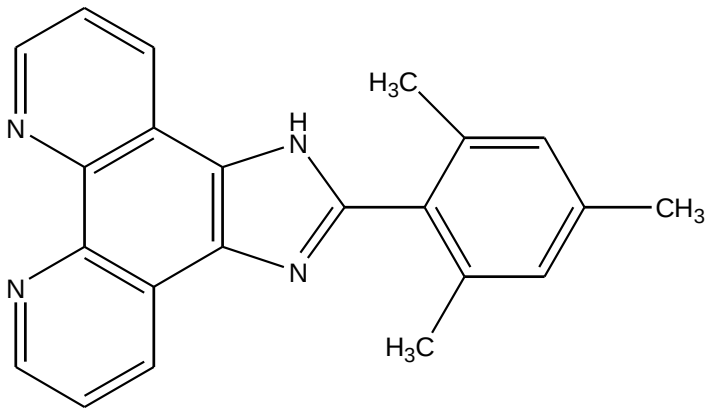

2-mesityl-1H-imidazo[4,5-f][1,10]phenanthroline **(G)**

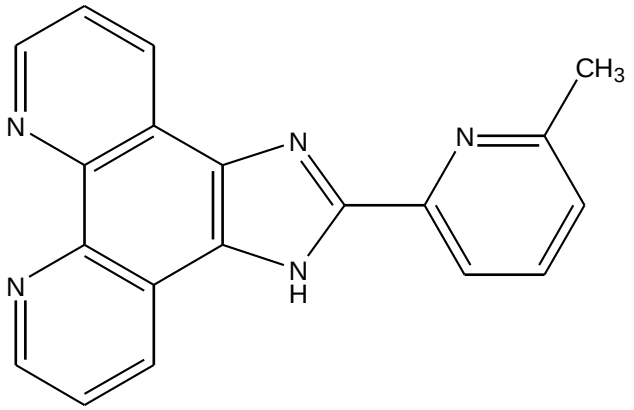

2-(6-methylpyridin-2-yl)-1H-imidazo[4,5-f][1,10]phenanthroline **(J)**

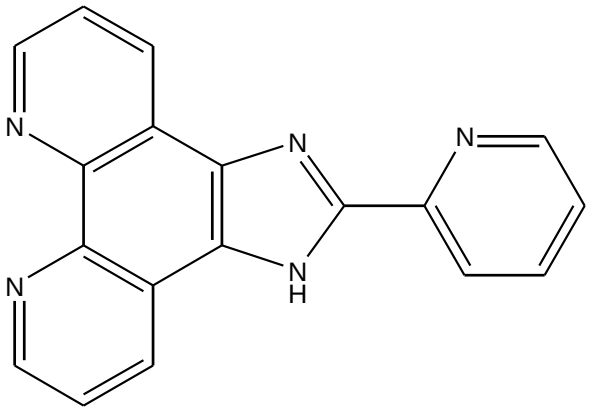

2-(pyridin-2-yl)-1H-imidazo[4,5-f][1,10]phenanthroline **(K)**

Figure 1. Names, molecular structures and the abbreviations of the inhibitors investigated.

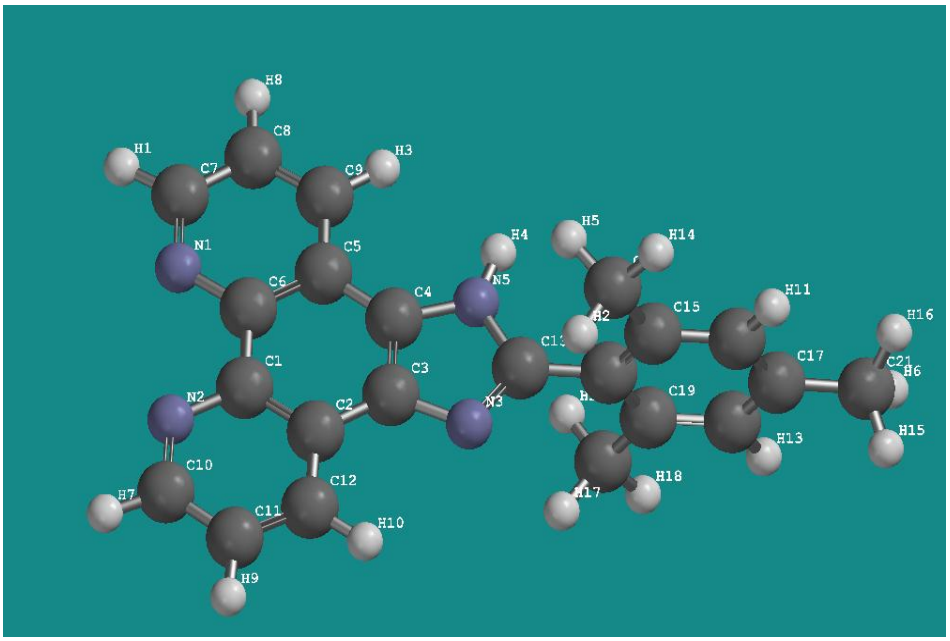

(G)

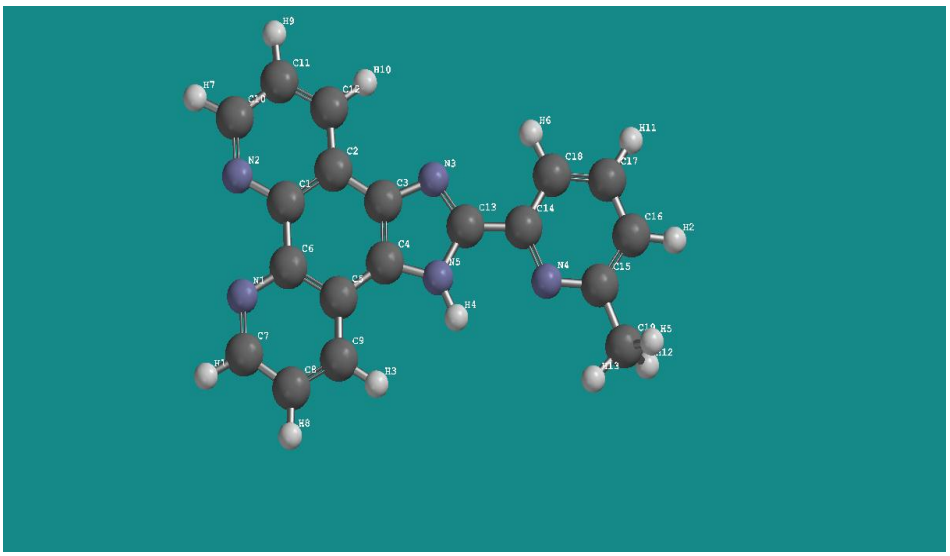

(J)

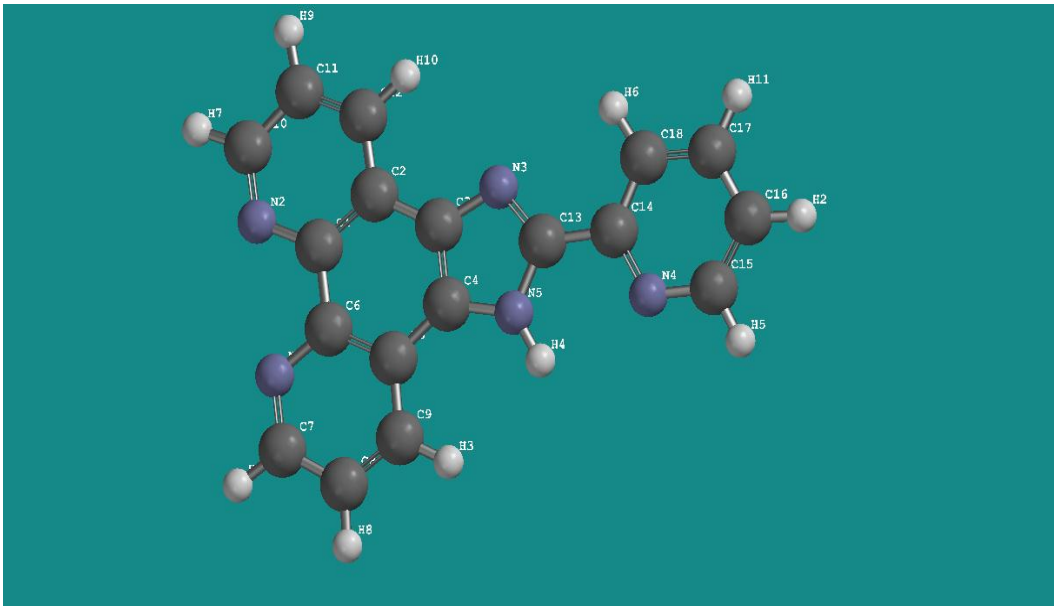

(K)

Figure 2. Optimized structure of G, J and K respectively (ball and stick model).

The chemical and optimized structures of the phenanthroline derivatives chosen for the study are presented in Figs. 1 and 2 respectively.

2. EXPERIMENTAL

2.1. General considerations

All starting materials were obtained commercially as reagent grade. All air or moisture sensitive manipulations were carried out under an atmosphere of nitrogen using standard Schlenk

techniques. All purifications were done on silica gel column to exclude impurities and TLC glass slides were routinely employed to monitor extents of reactions as well as the progess of silica gel column chromatography.

2.2. Synthesis of 2-mesityl-1H-imidazo [4,5-f][1,10] phenanthroline (G)

The inhibitor (MIP) was synthesized as reported in the literature [23]. 1,10-phenanthroline-5,6-dione (0.50 g, 2.37 mmol), mesitaldehyde (0.35 g, 2.37 mmol), ammonium acetate (3.65 g, 47.40 mmol) and glacial acetic acid (10 mL) were heated under reflux condition for 2 h followed by cooling; diluted in 20 mL of distilled water and neutralized with concentrated aqueous ammonia solution.

The crude product was filtered off as yellow precipitate which was recrystallized from ethanol to obtain 2-mesityl-1H-imidazo[4,5-f][1,10] phenanthroline (Scheme 1) as microcrystals (0.75 g, Yield : 93 %).

2.3 Synthesis of 2-(6-methylpyridin-2-yl)-1H-imidazo [4,5-f][1,10] phenanthroline(J)

Phenanthroline-5,6-dione (3.00 g, 0.014 mol) and ammonium acetate (22 g, 0.29 mol) were weighed into the reaction flask and then charged with nitrogen atmosphere. Ethanol (15 mL), dichloromethane (15 mL), catalytic amount of glacial acetic acid (0.5 mL) and 6-methylpyridine-2-carboxaldehyde (2.18 g, 18.01 mmol, 1.25 equivalent) were added and the mixture was refluxed for 3 h.

After cooling, the reaction mixture was neutralized by concentrated aqueous ammonia and the volume was reduced under pressure. The organic components were extracted using dichloromethane (50 mL, thrice). The organic extracts were combined, concentrated and purified on silica gel column using ethyl acetate/petroleum ether (1:4) to elute the product. Portions containing the products were concentrated and addition of petroleum ether gave 2-(6-methylpyridin-2-yl)-1H-imidazo[4,5-f][1,10] phenanthroline as light yellow micro-crystals.

2.4 Synthesis of 2-(pyridin-2-yl)-1H-imidazo[4,5-f][1,10]phenanthroline(K)

The reaction flask containing phenanthroline-5,6-dione (5.00g, 0.024 mol), ammonium acetate (37 g, 0.480 mol), glacial acetic acid as catalyst (1 mL) and 2-pyridinecarboxaldehyde (2.86 mL, 0.030 mol) were added and the mixture was refluxed for 3 hours.

After cooling, the reaction mixture was neutralized by concentrated aqueous ammonia and the volume was reduced under reduced pressure.

The organic components were extracted using chloroform (50 mL, thrice) and the crude mixture was purified on silica gel column using ethanol/ethylacetate/petroleum ether (1:10:10) as eluent. The portions that contained pure products were concentrated and the precipitates were filtered, washed with small amount of ethanol and dried to afford isolated products (2.60 g, 36.4 %).

2.5.Material

Tests were performed on a freshly prepared sheet of mild steel of the following composition (wt. %): 0.13% C, 0.18% Si, 0.39% Mn, 0.40% P, 0.04% S, 0.025% Cu, and bal Fe. Specimens used in the weight loss experiment were mechanically cut into 5.0 cm x 4.0 cm x 0.8 cm dimensions, then abraded with SiC abrasive papers 320, 400 and 600 grit respectively, washed in absolute ethanol and acetone, dried at room temperature and stored in a moisture free dessicator before their use in corrosion studies [2].

2.6. Solutions

The aggressive solutions, 0.5 M H_2SO_4 were prepared by dilution of analytical grade 98% H_2SO_4 with distilled water. Stock solution of MIP was made in 10:1 water: methanol mixture to ensure solubility [6]. This stock solution was used for all experimental purposes. The concentration range of MIP prepared and used in this study was 2 µM – 10 µM.

2.7. Gravimetric measurements

The gravimetric method (weight loss) is probably the most widely used method of inhibition assessment [4]. The simplicity and reliability of the measurement offered by the weight loss method is such that the technique forms the baseline method of measurement in many corrosion monitoring programmes [5]. Weight loss measurements were conducted under total immersion using 250 mL capacity beakers containing 200 mL test solution at 303 K maintained in a thermostated water bath. The mild steel coupons were weighed and suspended in the beaker with the help of rod and hook. The coupons were retrieved at 2 h interval progressively for 10 h, washed thoroughly in 20% NaOH solution containing 200 g/l of zinc dust with bristle brush, rinsed severally in deionized water, cleaned, dried in acetone, and re-weighed [2,3]. The weight loss (in grammes), was taken as the difference in the weight of the mild steel coupons before and after immersion in different test solutions. In order to get good reproducibility, experiments were carried out in triplicate. In this present study, the standard deviation values among parallel triplicate experiments were found to be smaller than 4%, indicating good reproducibility.

The corrosion rate ,ρ (in mg cm^{-2} h^{-1}) was calculated from the following equation [3]:

$$\rho = \frac{\Delta W}{St} \qquad (1)$$

where W is the average weight loss of three mild steel sheets, S the total area of one mild steel specimen, and t is the immersion time (10 h) . With the calculated corrosion rate, the inhibition efficiency (%I) was calculated as follows [23] :

$$\%I = \left(\frac{\rho_1 - \rho_2}{\rho_1} \right) x100 \quad (2)$$

Where ρ_1 and ρ_2 are the corrosion rates of the mild steel coupons in the absence and presence of inhibitor, respectively.

2.8. Computational details

B3LYP, a version of the DFT method that uses Becke's three parameter functional (B3) and includes a mixture of HF with DFT exchange terms associated with the gradient corrected correlation functional of Lee, Yang and Parr (LYP) [24], was used in this paper to carry out quantum calculations. Then, full geometry optimization together with the vibrational analysis of the optimized structures of the inhibitor was carried out at the B3LYP/6-31G (d) level of theory using Spartan'06 V112 program package [25] in order to determine whether they correspond to a maximum or a minimum in the potential energy curve. The quantum chemical parameters were calculated for molecules in neutral as well as in the protonated form for comparison. It is well known that the phenomenon of electrochemical corrosion occurs in liquid phase. As a result, it was necessary to include the effect of a solvent in the computational calculations. In the Spartan '06 V112 program, SCRF methods (Self-consistent reaction field) were used to perform calculations in aqueous solution. These methods model the solvent as a continuum of uniform dielectric constant and the solute is placed in the cavity within it.

There is no doubt that the recent progress in DFT has provided a very useful tool for understanding molecular properties and for describing the behaviour of atoms in molecules. DFT methods have become very popular in the last decade due to their accuracy and less computational time. Density functional theory has been found to be successful in providing insights into the chemical reactivity and selectivity, in terms of global parameters such as electronegativity (χ), hardness (η) and softness (σ), and local ones such as the Fukui function $(f(r))$ and local softness $(s(r))$. Thus, for an *N*-electron system with total electronic energy (*E*) and an external potential $(\nu(r))$; chemical potential (ρ) known as the negative of electronegativity (χ), has been defined as the first derivative of the *E* with respect *N* at $\nu(r)$ [26]:

$$\chi = -\rho = -\left(\frac{\partial E}{\partial N} \right)_{\nu(r)} \quad (3)$$

Hardness (η) has been defined within the DFT as the second derivative of the E with respect N at $\nu(r)$ property which measures both the stability and reactivity of a molecule [27]:

$$\eta = \left(\frac{\partial^2 E}{\partial N^2} \right)_{\nu(r)} = \left(\frac{\partial \rho}{\partial N} \right)_{\nu(r)} \quad (4)$$

where E is the electronic energy, N is the number of electrons, and $v(r)$ is the external potential due to the nuclei and ρ is chemical potential.

The number of transferred electrons (ΔN) from the inhibitor molecule to the metal surface can be calculated by using the following equation [28]:

$$\Delta N = \frac{\chi_{Fe} - \chi_{inh}}{[2(\eta_{Fe} + \eta_{Fe})]} \tag{5}$$

where χ_{Fe} and χ_{inh} denote the absolute electronegativity of iron and the inhibitor molecule, respectively; η_{Fe} and η_{inh} denote the absolute hardness of iron and the inhibitor molecule, respectively.

I and A are related in turn to E_{HOMO} and E_{LUMO} using the equations below [29]:

$$I = -E_{HOMO} \tag{6}$$

$$A = -E_{LUMO} \tag{7}$$

These quantities are related to electron affinity (A) and ionization potential (I) using the equation below:

$$\chi = \frac{I + A}{2}, \quad \chi = -\frac{E_{LUMO} + E_{HOMO}}{2} \tag{8}$$

$$\eta = \frac{I - A}{2}, \quad \eta = -\frac{E_{LUMO} - E_{HOMO}}{2} \tag{9}$$

Recently, a new global chemical reactivity parameter has been introduced and is called an electrophilicity index (ω). It is defined as [30]:

$$\omega = \frac{\rho^2}{2\eta} \tag{10}$$

This was proposed as a measure of the electrophilic power of a molecule. Global softness can also be defined as [31]:

$$\sigma = \frac{1}{\eta} \tag{11}$$

It is also important to consider the situation corresponding to a molecule that is going to receive a certain amount of charge at some center and is going to back-donate a certain amount of charge through the same center or another one. To describe the energy change associated with these two

processes, the second order simple charge transfer formula was regarded as a two-parameter expression, in which the donation and back-donation processes are differentiated through the use of the values of the chemical potential for each case, while the hardness is fixed to the value of $\eta = (\mu^+ - \mu^-)$ in both situations. Thus, according to the simple charge transfer model for donation and back-donation of charges proposed recently by Gomez et al., [32], when a molecule receives a certain amount of charge, ΔN^+;

$$\Delta E^+ = \mu^+ \Delta N^+ + \frac{1}{2}\eta(\Delta N^+)^2 \tag{12}$$

while when a molecule back-donates a certain amount of charge, ΔN^-, then:

$$\Delta E^- = \mu^- \Delta N^- + \frac{1}{2}\eta(\Delta N^-)^2 \tag{13}$$

If the total energy change is approximated by the sum of the contributions of Eqs. (12) and (13), and assuming that the amount of charge back-donation is equal to the amount of charge received, $\Delta N^- = -\Delta N^+$, then;

$$\Delta E_T = \Delta E^+ + \Delta E^- = (\mu^+ - \mu^-)\Delta N^+ + \eta(\Delta N^+)^2 \tag{14}$$

The most favorable situation corresponds to the case when the total energy change becomes a minimum with respect to ΔN^+, which implies that $\Delta N^+ = -(\mu^+ - \mu^-)/2\eta$ and that;

$$\Delta E_T = -(\mu^+ - \mu^-)^2 / 4\eta = -\eta / 4 \tag{15}$$

The local reactivity of the inhibitors was analyzed through an evaluation of the Fukui indices [33]. These are measurements of the chemical reactivity, as well as an indication of the reactive regions and the nucleophilic and electrophilic behavior of the molecule. The regions of a molecule where the Fukui function is large are chemically softer than the regions where the Fukui function is small, and by invoking the HSAB principle in a local sense, one may establish the behavior of the different sites with respect to hard or soft reagents. The Fukui function *f(r)* is defined as the first derivative of the electronic density *ρ(r)* with respect to the number of electrons *N* at a constant external potential *v(r)*. Thus, using a scheme of finite difference approximations from Mulliken population analysis of atoms in the inhibitors and depending on the direction of electron transfer we have [34-36]:

$$f_k^+ = q_k(N+1) - q_k(N) \qquad \text{(for nucleophilic attack)} \tag{16}$$

$$f_k^- = q_k(N) - q_k(N-1) \qquad \text{(for electrophilic attack)} \tag{17}$$

$$f_k^o = \frac{q_k(N+1) - q_k(N-1)}{2} \qquad \text{(for radical attack)} \qquad (18)$$

where q_k is the gross charge of atom *k* in the molecule i.e. the electron density at a point *r* in space around the molecule. *N* corresponds to the number of electrons in the molecule. *N+1* corresponds to an anion, with an electron added to the LUMO of the neutral molecule; N-1 corresponds to the cation with an electron removed from the HOMO of the neutral molecule. All calculations were done at the ground-state geometry. These functions can be condensed to the nuclei by using an atomic charge partitioning scheme, such as Mulliken population analysis in Eqs. (16) - (18).

3. RESULTS AND DISCUSSION

Experimentally, the order of the inhibition efficiencies of these inhibitors studied is K < J < G (Table 1).

Table 1. Experimental Inhibition efficiency obtained from gravimetric measurements at 303 K.

Inhibitor	Concentrations	Inhibition efficiency (*I*%)
G	2 x 10^{-6} M	52.0
4 x 10^{-6} M	60.0	
6 x 10^{-6} M	69.0	
8 x 10^{-6}M	75.0	
10 x 10^{-6}M	87.0	
J	2 x 10^{-6} M	39.0
4 x 10^{-6} M	50.0	
6 x 10^{-6} M	57.0	
8 x 10^{-6}M	60.0	
10 x 10^{-6}M	72.0	
K	2 x 10^{-6} M	30.0
4 x 10^{-6} M	40.0	
6 x 10^{-6} M	51.0	
8 x 10^{-6}M	60.0	
10 x 10^{-6}M	71.0	

It is predictable from the molecular structure of the studied inhibitors that 2-mesityl-1H-imidazo[4,5-f][1,10]phenanthroline (G) will have the highest inhibition efficiency. This is due to the presence, apart from the phenanthroline and imidazole moeity, of three methyl groups (-CH_3) attached to the aromatic ring in the molecule which can donate electrons thus increasing the reactivity of the molecule onto the steel surface. This is expected to overshadow the presence of aditional pyridine rings

on K and J. The adsorption of these inhibitors on steel surface may take place in the following ways [37]: (i) the inhibitor molecules may be adsorbed via donor-acceptor interactions between the π-electrons of the aromatic rings and unshared electron pairs of the heteroatoms to form a bond with the vacant d-orbitals of the metal surface (chemisorption). (ii) In acidic media, the N heteroatoms are readily protonated, which might adsorb onto the metallic surface via the negatively charged acid anion (SO_4^{2}) (physisorption). Thus physical and chemical adsorption will lead to the formation of protective films of the inhibitor molecules onto the steel surface. From the foregoing, it was pertinent to compute all the quantum chemical parameters both in the neutral forms and in the protonated forms in aqueous phase for comparison.

3.1. Quantum chemical study of neutral inhibitors

According to the frontier molecular orbital theory (FMO), the chemical reactivity is a function of interaction between HOMO and LUMO levels of the reacting species [38]. E_{HOMO} is a quantum chemical parameter which is often associated with the electron donating ability of the molecule. High value of E_{HOMO} is likely to indicate a tendency of the molecule to donate electrons to appropraite acceptor molecule of low empty molecular orbital energy [39]. Therefore, the energy of the lowest unoccupied molecular orbital, E_{LUMO}, indicates the ability of the molecule to accept electrons [40]. So, the lower the value of E_{LUMO}, the more probable the molecule would accept electrons. Thus the binding ability of the inhibitor to the metal surface increases with increasing of the HOMO and decreasing of the LUMO energy values. All the quantum chemical parameters/descriptors for the neutral form of the inhibitors are given in Tables 2.

Table 2. The calculated quantum chemical parameters for G, J, K in the neutral form obtained using DFT at the B3LYP/6-31G (d) basis set in aqueous phase.

Quantum chemical properties	G	J	K
Total energy (au)	-1068.25	-1005.68	-966.75
E_{HOMO} (eV)	-5.72	-5.58	-5.64
E_{LUMO} (eV)	-1.32	-1.56	-1.62
ΔE (eV)	4.40	4.02	4.02
Dipole moment (D)	5.64	6.04	5.56
Molecular weight (amu)	338.41	311.34	297.32
Molecular area ($Å^2$)	365.40	323.10	302.70
Molecular volume ($Å^3$)	354.01	311.64	293.25
Ionization potential (I) (eV)	5.72	5.58	5.64
Electron affinity (A) (eV)	1.32	1.56	1.62
Electronegativity (χ)	3.02	3.57	3.63
Hardness (η)	2.20	2.01	2.01
Softness (σ)	0.45	0.49	0.49
Fraction of electrons transferred (ΔN)	0.90	0.85	0.84
Neucleophilicity (ω)	2.07	3.15	3.26
ΔE_T	-0.55	-0.50	-0.50

According to Table 2, the total energy values which shows how stable the molecules are follow the trend K < J < G, which is the same order with the experimentally determined inhibition efficiency. The values of E_{HOMO} follow the order; G > K > J which does not correlate with the experimantally determine inhibition efficiency. The values of E_{LUMO} follow the order; G < J < K which deviates with the order of inhibition efficiency obtained experimentally.

The separation energy, $\Delta E = (E_{LUMO} - E_{HOMO})$, is an important parameter and it is a function of reactivity of the inhibitor molecule towards the adsorption on metallic surface. As ΔE decreases, the reactivity of the molecule increases leading to increase in the inhibition efficiency of the molecule [41]. The calculations from Table 2 show the decreasing trend for the property: G < J < K, which does not follow the same order of inhibition efficiency obtained for the inhibitors.

It is shown from the calculations that there was no obvious correlation between the values of the dipole moment with the trend of inhibition efficiency obtained experimentally. There is lack of agreement in the literature on the correlation between the dipole moment and inhibition efficiency [42, 43]. The B3LYP/6-31G (d) calculations showed an obvious correlation between the molecular weight, molecular volume and molecular area of the molecules and the inhibition efficiency. The inhibition efficiency increases as the molecular weight, molecular volume and the molecular area increases due to the increase of the contact area between molecule and surface. It is clear from Table 2 that G has the highest molecular weight, molecular volume and molecular area which probably increases it adsorption on the metal surface and increases the inhibition efficiency.

Absolute hardness, η and softness, σ are important properties to measure the molecular stability and reactivity. A hard molecule has a large energy gap and a soft molecule has a small energy gap. Soft molecules are more reactive than hard ones because they could easily offer electrons to an acceptor. For the simplest transfer of electrons, adsorption could occur at the part of the molecule where σ, which is a local property, has the highest value [44]. In a corrosion system, the inhibitor acts as a Lewis base while the metal acts as a Lewis acid. Bulk metals are soft acids and thus soft base inhibitors are most effective for acidic corrosion of these metals. It is shown from the calculations that G has the highest hardness and the lowest softness which deviates from the expected trend from the experimental inhibition efficiency obtained. Normally, the inhibitor with the least value of global hardness (hence the highest value of global softness) is expected to have the highest inhibition efficiency [45].

The number of electrons transferred (ΔN) was also calculated and tabulated in Table 2. Values of ΔN show that the inhibition efficiency resulting from electron donation agrees with Lukovits's study [28]. If $\Delta N < 3.6$, the inhibition efficiency increases by increasing electron-donating ability of these inhibitors to donate electrons to the metal surface and it increases in the following order: K < J < G. The results indicate that ΔN values correlates strongly with experimental inhibition efficiencies. Thus, the highest fraction of electrons transferred is associated with the best inhibitor (G), while the least fraction is associated with the inhibitor that has the least inhibition efficiency (K).

The electrophilicity index, ω, which shows the ability of the inhibitor molecules to accept electrons follow the trend: G < J < K. Thus, G exhibits the lowest value of electrophilicity (Table 2) which confirms its lowest capacity to accept electrons. Thus, there is no correlation between this property and inhibition efficiency.

The calculations from Table 2 indicate that $\eta > 0$ (η = hardness), $\Delta E_T < 0$ (as also obtained in this study). This result implies that the charge transfer to a molecule followed by back-donation from the molecule is energetically favorable. Similar observation has been reported [32]. However, it is important to note that Eq. (13) does not predict that a back-donation process is going to occur; it only establishes that if both processes occur (charge transfer to the molecule and back-donation from the molecule), the energy change is directly proportional to the hardness of the molecule. In this context, Eq. (13) may be useful for a family of similar molecules (like the one in this study), which are known to back-donate the charge they receive, because then the stabilization will increase as the hardness increases among the members of the family, given that they are interacting with the same metal surface. If it is assumed that the inhibition efficiency (*I %*) should increase when there is a better adsorption of the molecule on the metal surface, then the (*I%*) should increase when the stabilization energy that results from the interaction between the metal surface and inhibitor increases. Thus, taking into account that the interaction of this type of molecules with the metal surfaces occurs, in general, through donation and back-donation, then according to Eq.(13), the total energy change values calculated (Table 2) is in the order G < J = K which does not support the order obtained for the inhibition efficiencies.

3.2. Quantum chemical study of protonated inhibitors

Organic inhibitors under investigation have a great tendency to be protonated in acidic medium due to the presence of several N atoms. This is confirmed from the calculations which show the great stability of protonated inhibitors (high negative total energies Table 3).

Table 3. The calculated quantum chemical parameters for G, J, K in the protonated form obtained using DFT at the B3LYP/6-31G (d) basis set in aqueous phase.

Quantum chemical properties	G	J	K
Total energy (au)	-1068.63	-1006.07	-996.75
E_{HOMO} (eV)	-9.50	-9.52	-9.60
E_{LUMO} (eV)	-5.86	-6.20	-6.29
ΔE (eV)	3.64	3.32	3.30
Dipole moment (D)	3.89	6.25	8.90
Molecular weight (amu)	339.42	312.34	298.32
Molecular area ($Å^2$)	368.95	327.30	306.94
Molecular volume ($Å^3$)	357.26	315.12	296.76
Ionization potential (I) (eV)	9.50	9.52	9.60
Electron affinity (A) (eV)	5.86	6.20	6.29
Electronegativity (χ)	7.68	7.86	7.95
Hardness (η)	1.82	1.66	1.65
Softness (σ)	0.55	0.60	0.60
Fraction of electrons transferred (ΔN)	-0.186	-0.260	-0.280
Neucleophilicity (ω)	16.20	18.61	18.20
ΔE_T	-0.45	-0.42	-0.41

It is shown from the optimized structures of the investigated inhibitors, that there is one or more active center on the inhibitor for protonation.

Comparison of quantum chemical calculations for protonated and neutral inhibitors indicates that there is a clear correlation between most of the quantum chemical parameters/descriptor in the protonated form and the corrosion inhibiting effect of the inhibitors than in the neutral form (Table 3).

Most of the quantum chemical parameters/descriptors calculated in the protonated form such as total energy, E_{HOMO}, molecular weight, molecular area, molecular volume, hardness, softness, fraction of electrons transferred and total energy change, were in accordance with the order of inhibition efficiency obtained experimentally: K < J < G. However, there was lack of correlation between quantum chemical parameters such as E_{LUMO}, separation energy, $\Delta E = (E_{LUMO} - E_{HOMO})$, dipole moment and electrophilicity index with the order of inhibition efficiency obtained experimentally. These results demonstrate that in acid medium, the protonated form of the inhibitors should make a higher contribution to the corrosion inhibiting effect of the inhibitors on mild steel.

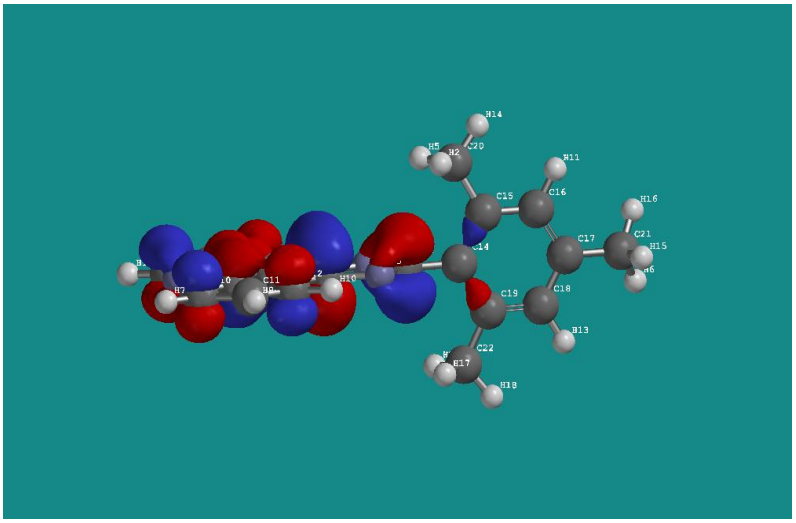

(G)

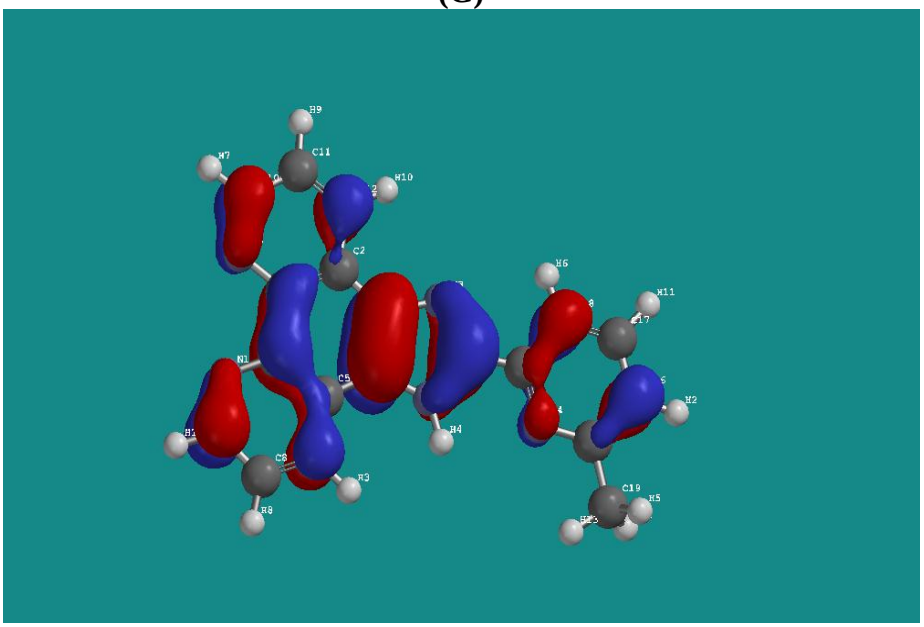

(J)

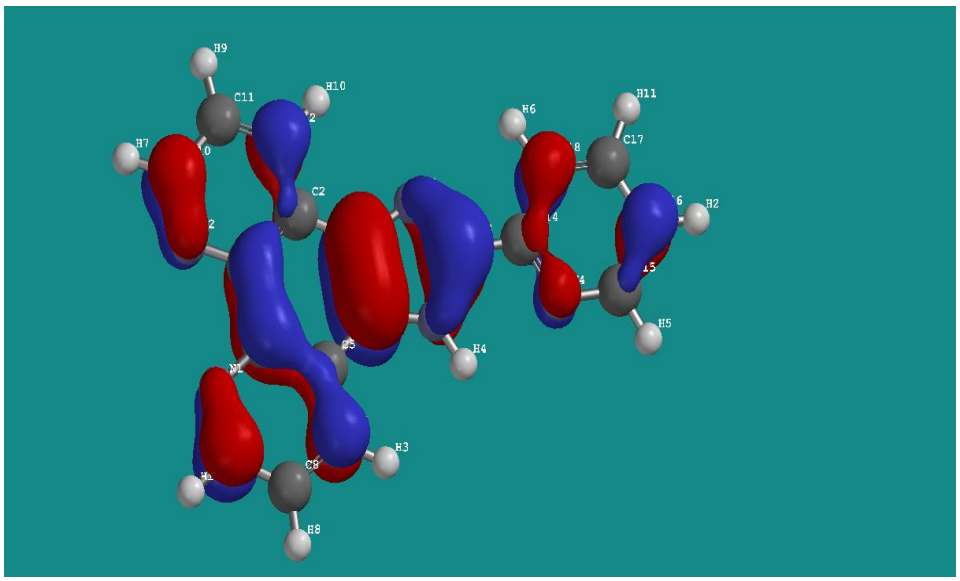

(K)

Figure 3a. The highest occupied molecular orbital (HOMO) of G, J and K respectively using DFT at the B3LYP/6-31G (d) basis set level in the neutral form.

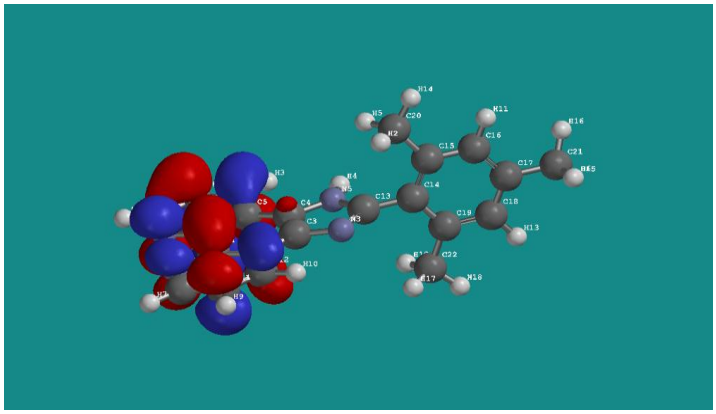

(G)

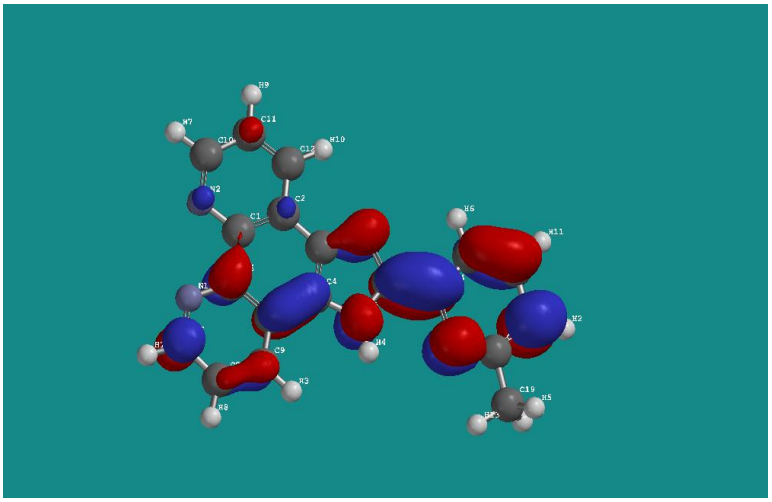

(J)

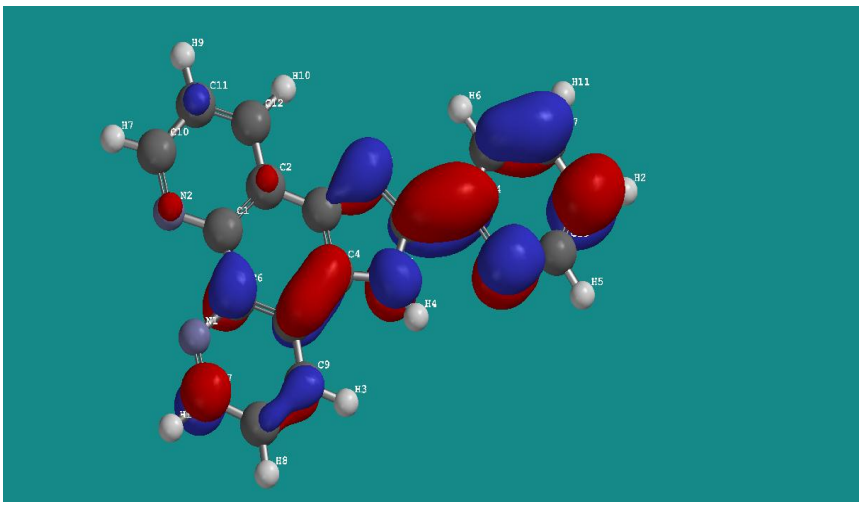

(K)

Figure 3b. The lowest unoccupied molecular orbital (LUMO) of G, J and K respectively using DFT at the B3LYP/6-31G (d) basis set level in the neutral form.

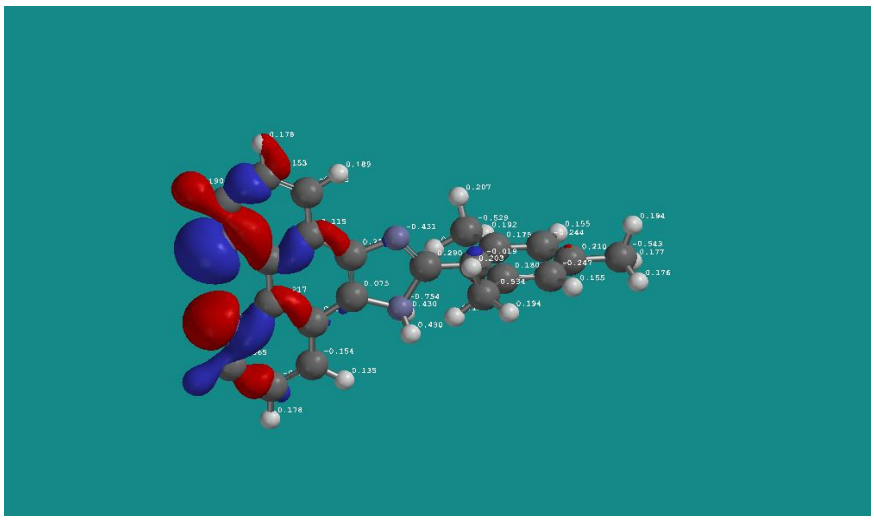

(G)

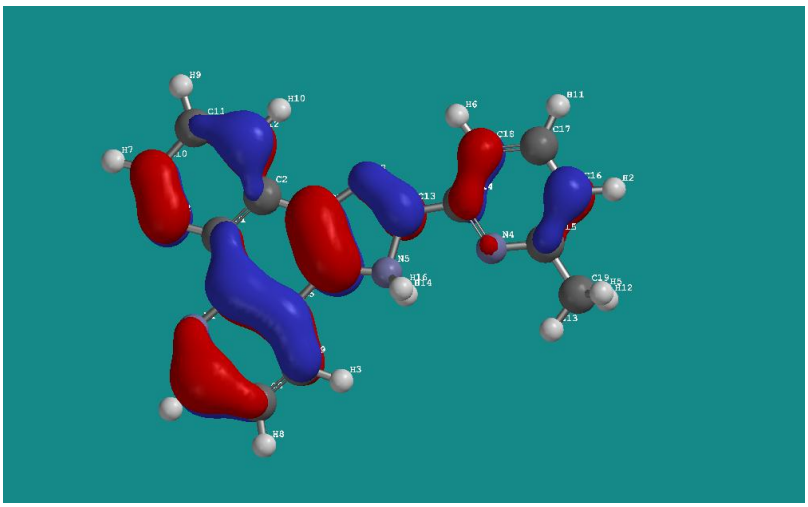

(J)

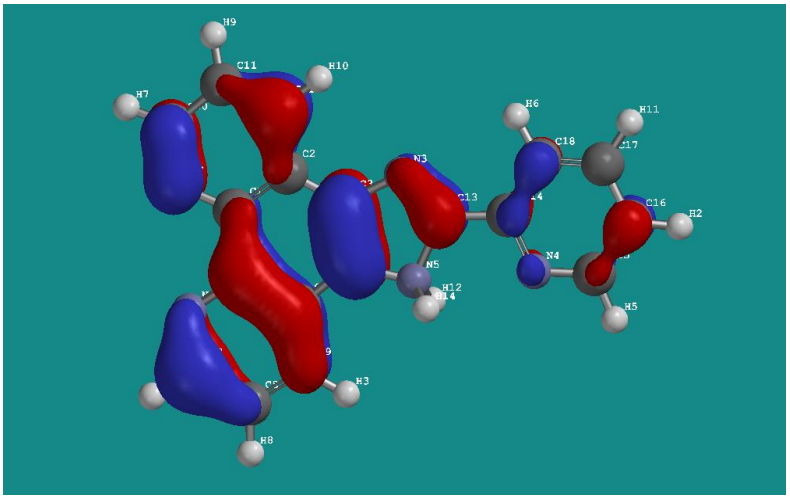

(K)

Figure 4a. The highest occupied molecular orbital (HOMO) of G, J and K respectively using DFT at the B3LYP/6-31G (d) basis set level in the protonated form.

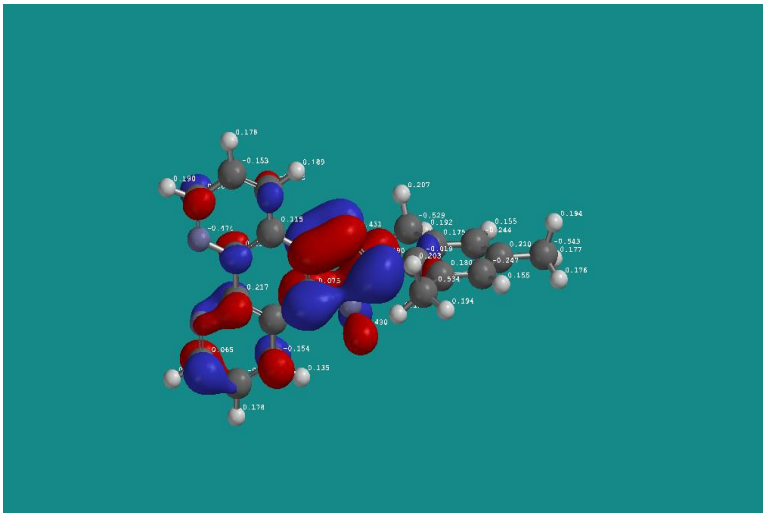

(G)

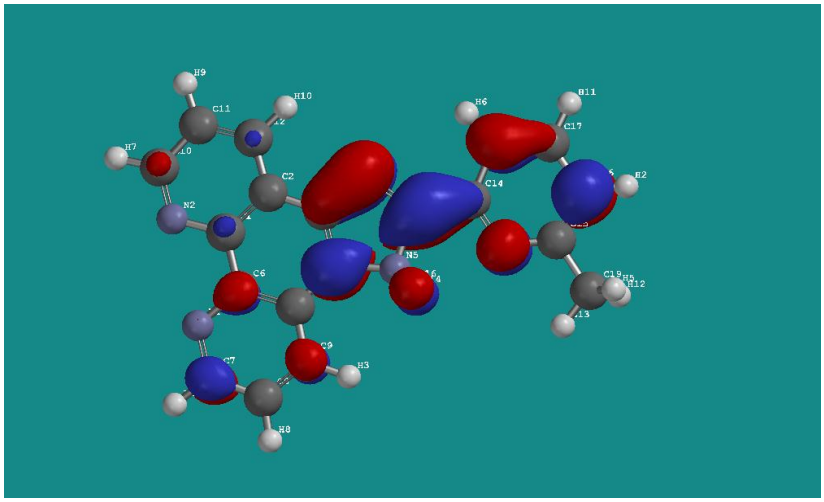

(J)

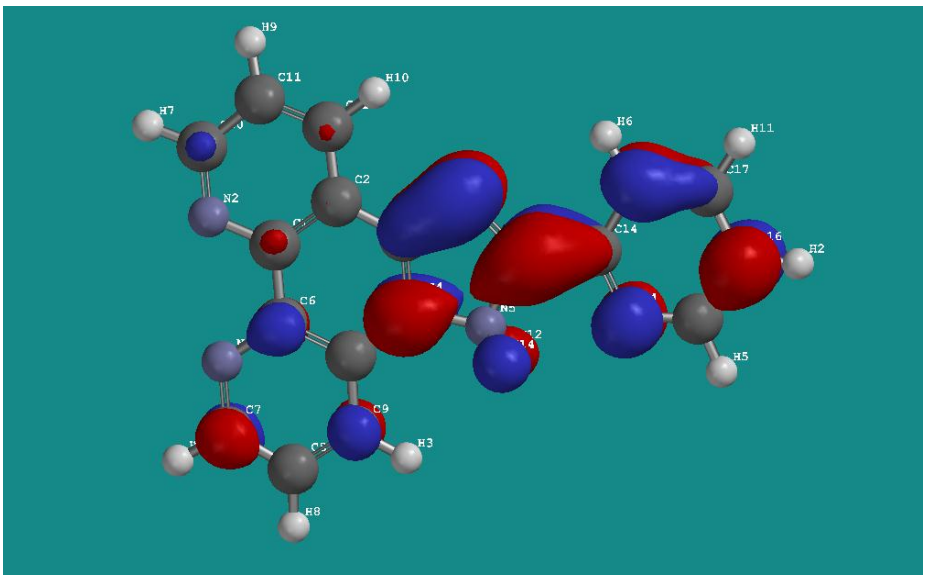

(K)

Figure 4b. The lowest unoccupied molecular orbital (LUMO) of G, J and K respectively using DFT at the B3LYP/6-31G (d) basis set level in the protonated form.

Figures 3 and 4 show the HOMO and LUMO orbital contributions for the neutral and protonated species of the studied molecules respectively. For molecule G, The HOMO densities were concentrated on both the phenanthroline and the imidazole rings in the neutral form while the protonated form has the HOMO mainly in the phenanthroline ring. For the LUMO distributions of molecule G, the reverse is the case. In the case of molecules J and K, both the HOMO and the LUMO distributions were partition throughout the entire molecules in both the neutral and the protonated forms.

Thus, unoccupied d orbitals of Fe atom can accept electrons from inhibitor molecule both in the neutral and protonated species to form a coordinate bond. Also the inhibitor molecule can accept electrons from Fe atom with its anti-bonding orbitals to form back-donating bond.

These donation and back-donation processes strengthen the adsorption of these inhibitors onto the mild steel surface

3.3. Mulliken atomic charges and Fukui functions

The use of Mulliken population analysis to estimate the adsorption centers of inhibitors has been widely reported and it is mostly used for the calculation of the charge distribution over the whole skeleton of the molecule [46].

There is a general consensus by several authors that the more negatively charged heteroatom is, the more is its ability to adsorb on the metal surface through a donor-acceptor type reaction [2, 3, 5]. The Mulliken charge distributions of the studied compounds together with the calculated Fukui indices are presented in Tables 4-6. The parameters were calculated for the heteroatoms only for simplicity.

Table 4. Calculated Mulliken atomic charges and Fukui functions for heteroatoms of G using DFT at the B3LYP/6-31G (d) basis set.

Atom	q_N	q_{N+1}	q_{N-1}	f_k^+	f_k^-
N1	-0.483	-0.469	-0.535	0.014	0.052
N2	-0.489	-0.475	-0.528	0.014	0.039
N3	-0.555	-0.574	-0.571	-0.019	0.016
N4	-0.732	-0.760	-0.733	-0.028	0.001

Table 5. Calculated Mulliken atomic charges and Fukui functions for heteroatoms of J using DFT at the B3LYP/6-31G (d) basis set.

Atom	q_N	q_{N+1}	q_{N-1}	f_k^+	f_k^-
N1	-0.475	-0.457	-0.486	0.018	0.011
N2	-0.482	-0.465	-0.500	0.017	0.018
N3	-0.592	-0.567	-0.630	0.025	0.038
N4	-0.588	-0.582	-0.623	0.006	0.035
N5	-0.769	-0.764	-0.793	0.005	0.024

Table 6. Calculated Mulliken atomic charges andFukui functions for heteroatoms of K using DFT at the B3LYP/6-31G (d) basis set.

Atom	q_N	q_{N+1}	q_{N-1}	f_k^+	f_k^-
N1	-0.475	-0.457	-0.486	0.018	0.011
N2	-0.481	-0.464	-0.500	0.017	0.019
N3	-0.593	-0.566	-0.631	0.027	0.038
N4	-0.529	-0.520	-0.568	0.009	0.039
N5	-0.770	-0.765	-0.792	0.005	0.022

The tables show that all the nitrogen atoms have high negative charge densities implying that the most probable reactive site for the adsorption of these inhibitors on mild steel surface is located on these atoms.

For a finite system such as an inhibitor molecule, when the molecule is accepting electrons one has f_k^+, the index for nucleophilic attack; when the molecule is donating electrons, one has f_k^-, the index for electrophilic attack. It is possible to observe from Tables 4-6 that N4, N3, N5; N3, N4, N5; and N1, N2, N3 are the most susceptible sites for electrophilic attacks for K, J and G molecules respectively. These sites present the highest values of f_k^-. On the other hand N3, N1, N2; N3, N1, N2; N1, N2 are the most susceptible sites for nucleophilic attacks for K, J and G respectively. These sites have the highest values of f_k^+. These results confirm the possibility of donation and back-donation of electrons between the inhibitors and the mild steel.

3.4. Quantitative structure and activity relationship (QSAR) consideration

In this investigation, quantitative structure and activity relationship (QSAR) has also been used to correlate the inhibition efficiency of the studied inhibitors and their molecular structure for both the neutral and protonated species. An attempt to correlate the quantum chemical parameters with the average experimental inhibition efficiencies showed that no simple relation or no direct trend relationship can be derived with the inhibition performance of these inhibitors. This is due to the complex interactions that are involved in the corrosion protection. Though a number of satisfactory correlations have been reported by other investigators [47-49] between the inhibition efficiency of various inhibitors used and some quantum chemical parameters, a composite index and a combination of more than one parameter [50, 51] has been used to perform QSAR which might affect the inhibition efficiency of the studied molecules. Consequently, a relation may exist between the composite index and the average corrosion inhibition efficiency for a particular inhibitor molecule. Therefore, in the present study, mathematical models were tentatively fitted to the experimental values of the inhibition efficiency, *I*%. The objectives were:

(1) To obtain equations useful in predicting *I*% from the concentrations of the inhibitors and their quantum chemical parameters.

(2) To provide theoretical explanations for the effects of the different variables studied.

The first model investigated is an empirical linear model expressed as:

$$I(\%) = B_1X_1 + B_2X_2 + ... + B_nX_n \tag{19}$$

where B_i are constants obtained by regression analysis; X_j are the independent variables consisting of quantum chemical values (E_{HOMO}, E_{LUMO}, ΔE, and D) and the inhibitor concentration (C_i, μM).

The experimental results were fitted to the empirical model of Eq. (19) by forward multiple linear-regression with switching, using the software package NCSS [52]. The size of the selected subset of independent variables was limited to include only the variables that are significant at the 0.05 level.

The estimated equations when using the quantum chemical values of the neutral and protonated molecules are:

Neutral: $$I\% = 4.390C_i - 19.26E_{HOMO} + 51.27E_{LUMO} \tag{20}$$

R^2= 0.9983 *SSE*=89.30

Protonated: $$I\% = 4.370C_i + 14.32\Delta E - 2.674D \tag{21}$$

R^2= 0.9986 *SSE*=77.27

where R^2 is the coefficient of determination, and *SSE* is the sum of squared errors defined as:

$$SSE = \sum (I\%_{experimental} - I\%_{estimated})^2 \tag{22}$$

Equations (20 and 21) produce close estimates of *I*%, Eq. 21 being slightly better. Both equations are useful in predicting the inhibition efficiency. Fig. 5 is a plot of the estimated versus the experimental *I*% values and it can be seen that the estimates are close to the experimental values. An inspection of the residual plots (not shown) did not suggest obvious deviation from homoscedasticity (constant variance). The normal probability plot of the regression residuals of Eq. 21 is shown in Fig. 6. The residuals seem to be normally distributed judging by their approximate linearity and by being enclosed inside the 95% confidence interval.

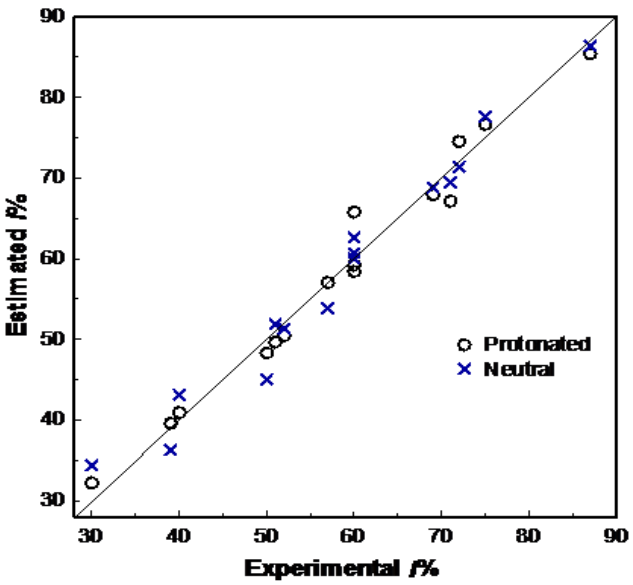

Figure 5. A plot of the *I*% values obtained from experiments versus *I*% values predicted from Equations 20 and 21.

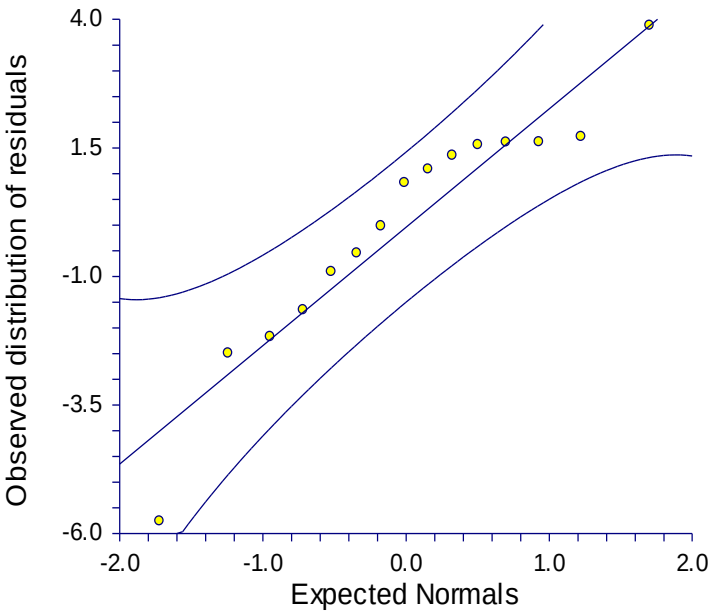

Figure 6. Normal probability plot of the residuals of fitting the experimental results to Eq. 21.

Another essential step in regression analysis is testing for multicollinearity. To test whether the selected independent variables are mutually interrelated or not, the correlation coefficients of variables and their relevant variance inflation factor (*VIF)* values were calculated. The outcomes showed that Eq. (20 and 21) cleared up the possibility. The calculation results for variables used in Eq. 21 are listed in Table 7.

Table 7. Correlation Matrix for the independent variables, and the variance inflation factor (*VIF*) and condition number (*CN*) of variables from Equation 21.

	C_i	ΔE	D	E_{HOMO}	E_{LUMO}	$I\%$	*VIF*	*CN*
C_i	1.0000	0.0000	0.0000	0.0000	0.0000	0.8427	0.9983	1.000
ΔE	0.0000	1.0000	-0.8754	0.6934	0.9892	0.5068	0.0247	1.875
D	0.0000	-0.8754	1.0000	-0.9553	-0.9369	-0.5006	0.7964	15.049
E_{HOMO}	0.0000	0.6934	-0.9553	1.0000	0.7916	0.4363	-	-
E_{LUMO}	0.0000	0.9892	-0.9369	0.7916	1.0000	0.5186	-	-
$I\%$	0.8427	0.5068	-0.5006	0.4363	0.5186	1.0000	-	-

Similar results (not shown) were obtained for Eq. 20. It can be seen in Table 7 that the values of some of the candidate independent variables are highly correlated; D has correlation coefficients of -0.9553 and -0.9369 with E_{HOMO} and E_{LUMO}, respectively. Also, the correlation of ΔE with E_{LUMO} is 0.9892. If any pair of these highly correlated variables is present in the model, their muticollinearity makes them redundant, and consequently, makes it difficult to assess partial effects of each independant variable. The selected independent variables in Eq. 21 are C_i, ΔE, and D and all their intercorellations are less than 0.9. Moreover, all calculated *VIF* values are less than 10 and condition number (*CN)* values less than 100, thus corroborating the absence of multicolliniarity in the empirical model of Eq. 21.

Both models of Eq. (20 and 21) passed the basic tests of regression analysis, so besides being useful for predicting $I\%$ values, theoretical conclusions can also be attempted for the effects of the independent variables in these models. The first thing to notice is the remarkable agreement in the coefficient of C_i in the two models, 4.390 and 4.370 for neutral and protonated quantum values, respectively. Eq. 20 states that $I\% = f\,(C_i, E_{HOMO}, E_{LUMO})$ while Eq 21 suggests that $\%I = f\,(C_i, \Delta E, D)$ and at face value this would seem like a discrepancy. However, examining the values in Table 7 shows that the correlation between ΔE and E_{LUMO} is 0.9892, almost a perfect linear correlation. Similarly the correlation between D and E_{HOMO} is -0.9553. The fact that Eq. 21 is a function of (C_i, ΔE, D) is a result of the mathematical method of variable selection. It is well known that in many cases, especially when some independent variables are highly correlated, the set of variables selected by forward multiple regression is not necessarily the same as backward multiple regression. Moreover, the algorithm of simple forward or backward regression may choose a set of variables that are not the same choice of stepwise regression. In other words, the present calculations leading to Eq. 21 selected the variables that best improved the probability function as the steps of the algorithm were executed.

To illustrate, the data used for building the model of Eq. 21 were fitted, by simple multiple regression, to a linear model using only the same variables in Eq. 20, the following equation was obtained:

Protonated: $$I\% = 4.387C_i - 33.14E_{HOMO} + 46.48E_{LUMO} \quad (23)$$

R^2= 0.9982 *SSE*=95.92

It was found, therefore, that replacing the variables ΔE and D with E_{HOMO} and E_{LUMO} resulted in a very small loss in the accuracy of estimates reflected in decreasing R^2 from 0.9986 to 0.9982 for the models of Eq. (21 and 23), respectively. This is not surprising because the two sets of variables are highly correlated as mentioned earlier, meaning that they can be used in the model interchangeably with little effect on the outcome of the equation. Accordingly, it can be concluded that, in the present family of inhibitors, I% can be accurately predicted from a knowledge of either (C_{i}, E_{HOMO}, E_{LUMO}) or (C_{i}, ΔE, D).

Besides the linear model of Eq. (19), there is also a nonlinear model that is commonly applied in corrosion inhibition studies. This nonlinear model was first proposed by Lukovits et al. [53] for the interaction of corrosion inhibitors with metal surfaces in acidic solutions. It has a theoretical derivation based on Langmuir adsorption isotherm, and is expressed as:

$$I(\%) = \frac{(AX_i + B)C_i}{1 + (AX_i + B)C_i} \times 100 \quad (24)$$

where A and B are constants obtained by regression analysis; X_{j} a quantum chemical index (E_{HOMO}, E_{LUMO}, ΔE, D) characteristic for the molecule; C_{i} is the inhibitor concentration in μM.

The estimated equations when using the quantum chemical values of the neutral and of the protonated molecules are:

Neutral: $$I\% = \frac{(-0.5973 - 2.807E_{HOMO} + 0.4644E_{LUMO} + 0.2757\Delta E + 0.004942D) \times C_i \times 100}{1 + (-0.5973 - 2.807E_{HOMO} + 0.4644E_{LUMO} + 0.2757\Delta E + 0.004942D) \times C_i} \quad (25)$$

R^2= 0.9302 *SSE*=226.65

Protonated: $$I\% = \frac{(1.402 + 0.2253E_{HOMO} - 0.09538E_{LUMO} + 0.4833\Delta E - 0.04617D) \times C_i \times 100}{1 + (1.402 - 0.2253E_{HOMO} - 0.09538E_{LUMO} + 0.4833\Delta E - 0.04617D) \times C_i} \quad (26)$$

R^2= 0.9301 *SSE*=226.74

The *SSE* of the nonlinear model is more than double the *SSE* of the linear models (Eq. 23, 25, and 26) which indicates that the linear models fit the data better.

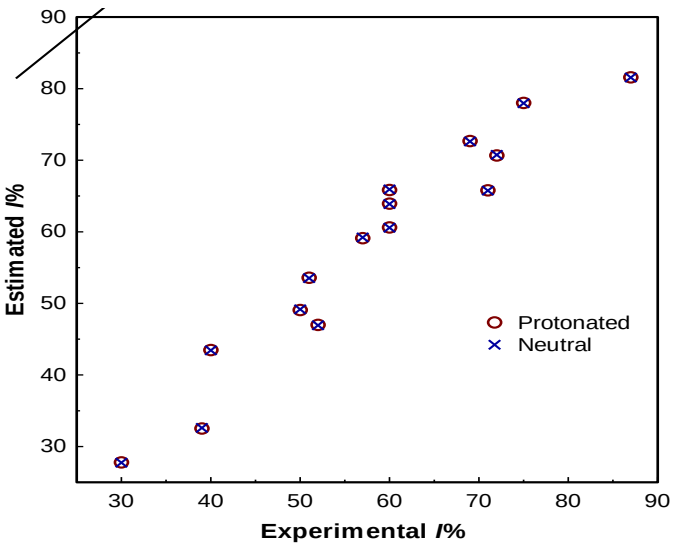

Figure 7. A plot of *I*% values obtained from experiments versus *I*% values predicted from Equations 23 and 24.

An inspection of Fig. 7 shows that Eqs. 25 and 26 estimated almost identical values of *I*%. Table 8 is the asymptotic correlation matrix of parameters estimated in Eq 24, it is clear that the parameters are very highly correlated, probably due to the multicollinearity of variables proved in Table 7. As a result, the asymptotic confidence intervals of regression parameters, listed in Table 9, are all wide and embrace zero, making the significance of the parameters questionable.

Table 8. Asymptotic correlation matrix of parameters estimated in Equation 24.

	C_i	ΔE	D	E_{HOMO}	E_{LUMO}
C_i	1.0000	-0.9997	-0.9999	0.9999	0.9997
ΔE	-0.9997	1.0000	0.9998	-0.9998	-0.9993
D	-0.9999	0.9998	1.0000	-0.9999	-0.9995
E_{HOMO}	0.9999	-0.9998	-0.9999	1.0000	0.9996
E_{LUMO}	0.9997	-0.9993	-0.9995	0.9996	1.0000

Table 9. Parameters estimated in Equation 26 and their standard errors.

Parameter Name	Parameter Estimate	Asymptotic Standard Error	Lower 90% Confidence Limit	Upper 90% Confidence Limit
C_i	1.4018	214.5791	-387.5146	390.3182
ΔE	0.2253	11.9705	-21.47087	21.92153
D	0.4832	33.4786	-60.1954	61.16197
E_{HOMO}	0.0953	35.6620	-64.54073	64.73148
E_{LUMO}	0.04617	0.6034	-1.098299	1.089065

The defects in the nonlinear models of Eq. (25 and 26) might be mitigated if the independent variables were selected to be free from multicollinearity. Therefore, with the aid of values in Table 7, the set of independent variables was selected to be (C_i, E_{HOMO}, E_{LUMO}). Another reasonable selection would be (C_i, ΔE, D), and it was seen in the previous analysis of the linear models that the two sets lead to almost the same results.

The estimated equations when using the selected set of variables (C_i, E_{HOMO}, E_{LUMO}) of the neutral and of the protonated molecules are:

Neutral: $$I\% = \frac{(2.633 + 0.1815E_{HOMO} + 0.8772E_{LUMO}) \times C_i \times 100}{1 + (2.633 + 0.1815E_{HOMO} + 0.8772E_{LUMO}) \times C_i} \quad (27)$$

R^2= 0.9285 SSE=231.97

Protonated: $$I\% = \frac{(5.685 + 0.2216E_{HOMO} + 0.5358E_{LUMO}) \times C_i \times 100}{1 + (5.685 + .2216E_{HOMO} + 0.5358E_{LUMO}) \times C_i} \quad (28)$$

R^2= 0.9280 SSE=233.67

The R^2 and SSE values deteriorated very slightly when the selected set of variables, (C_i, E_{HOMO}, E_{LUMO}), was used in modeling instead of the complete set (C_i, E_{HOMO}, E_{LUMO}, ΔE, D), thus providing more evidence to corroborate that some variables are redundant. Moreover, the standard errors of estimated parameters decreased by two orders of magnitude for the selected set of variables as shown in Table 10, thus improving the significance of estimates. However, the goodness of fit of the linear models is always higher than the nonlinear models investigated in the present study.

Table 10. Parameters estimated in Equation 28 and their standard errors.

Parameter Name	Parameter Estimate	Asymptotic Standard Error	Lower 90% Confidence Limit	Upper 90% Confidence Limit
C_i	5.6846	0.8255	4.2132	7.1559
E_{HOMO}	0.2216	0.1623	-0.0676	0.5109
E_{LUMO}	0.5358	0.1467	0.2743	0.7972

4.CONCLUSIONS

2-mesityl-1H-imidazo[4,5-f][1,10] phenanthroline (G), 2-(6-methylpyridin-2-yl)-1H-imidazo[4,5-f][1,10]phenanthroline (J) and 2-(pyridine-2-yl)-1H-imidazo[4,5-f][1,10]phenanthroline (K) have been found to be effective inhibitors for the corrosion of mild steel in acidic medium. Quantum chemical parameters such as E_{HOMO}, E_{LUMO}, energy of the gap, (ΔE), Dipole moment (D), hardness, softness, electrophilicity index, fraction of electrons transferred, charges etc. were calculated

using the density functional theory at B3LYP/6-31G (d) basis set and were correlated with the inhibition efficiencies of the inhibitors investigated. Our analysis have shown that one quantum chemically derived parameter is not sufficient in correlating the inhibitive ability of these types of compounds but several or a composite index of more than two or more parameters should be taken into consideration. The multiple-linear regression analyses fitted the theoretical data well and the calculated inhibition efficiency of the compounds studied was found to be close to their experimental corrosion inhibition efficiencies especially in the protonated form (R^2 = 0.9986). The results obtained in this study indicated that indeed, in acidic media, one should consider the protonated species involved because they seem to represent better the actual experimental situation. The QSAR approach is adequately sufficient to forecast the inhibitor efficiencies using the theoretical approach.

ACKNOWLEDGMENTS
Authors would like to appreciate the financial support from the University of Uyo during the period that this research was conducted and one of the authors Prof. M. I. El-Khaiary for carrying out the statistical analysis. E.E.E. acknowledges the National Research Foundation (NRF) of South Africa for funding.

References

1. A.Kokalj, *Electrochim. Acta* 56(2010) 745.
2. I.B. Obot, N.O. Obi-Egbedi, N.W. Odozi, *Corros. Sci.* 52 (2010) 923.
3. I.B. Obot, N.O. Obi-Egbedi, *Corros. Sci.* 52 (2010) 282.
4. I.B. Obot, N.O. Obi-Egbedi, *Surf. Rev. Lett.* 15(6) (2008) 903.
5. I.B. Obot, N.O. Obi-Egbedi, *Colloids and Surfaces A: Physicochem.Eng. Aspects*. 330 (2008) 207.
6. E.E. Ebenso, H. Alemu, S.A. Umoren, I.B. Obot, *Int. J. Electrochem. Sci*. 4 (2008) 1325.
7. M.M. El-Naggar, *Corros sci.* 49 (2007) 2236.
8. S.A. Umoren, E.E. Ebenso, *Mater. Chem. Phys*. 106 (2007) 393.
9. M. Lebrini, F. Bentiss, H. Vezin, M. Lagrenee, *Corros. Sci*. 48 (2006) 1291.
10. F. Bentiss, M. Traisnel, M. Lagrenee, *Appl. Surf. Sci.* 161 (2000) 196.
11. A.K. Singh, M.A. Quraishi, *Corros. Sci.* 52 (2010) 152.
12. A.S. Fouda, A.A. Al-Sarawy, E.E. El-Katori, *Desalination* 201 (2006) 1.
13. E.A. Noor, A.H. Al-Moubaraki, *Mater. Chem. Phys*. 110 (2008) 145.
14. F.S. de Sauza, A. Spinelli, *Corros. Sci.* 51 (2009) 642.
15. X. Li, S. Deng, H. Fu, T. Li, *Electrochimica Acta* 54 (2009) 4089.
16. X. Li, S. Deng, H. Fu, G. Mu, *Corros. Sci.* 51 (2009) 620.
17. A.Popova, E. Sokolova, M. Christov, *Corros. Sci.* 45 (2003) 33.
18. E.A. Noor, A.H. Al-Moubaraki, *Mater. Chem. Phys*. 110 (2008) 145.
19. G. Gece, Corros. Sci. 50 (2008) 298.
20. G. Bereket, C. Ogretir, A.Yurt, *J. Mol. Struct*. (THEOCHEM) 571 (2001) 13.
21. M.K. Awad, *J. Electroanal. Chem*. 567 (2004) 219.
22. M.K. Awad, F.M. Mahgoub, M.M. El-iskandrani, *J. Mol. Struct*. (THEOCHEM) 531 (2000) 105.
23. I.B. Obot, N.O. Obi-Egbedi, *Corros. Sci.* 52 (2010) 657.
24. C. Lee, W. Yang, R.G. Parr, *Phys. Rev. B37* (1988) 785.
25. Spartan,06 Wavefunction, Inc. Irvine, CA: Y. Shao, L.F. Molnar, Y. Jung, J. Kussmann, C. Ochsenfeld, S.T. Brown, A.T.B. Gilbert, L.V. Slipehenko, S.V. Levehenko, D.P. O'Neill, R.A. DiStasio Jr., R.C. Lochan, T.Wang, G.J.O. Beran, N.A. Besley, J.M. Herbert, C.Y. Lin, T. Van

Voorhis, S.H. Chien, A. Sodt, R.P. Steele, V.A. Rassolov, P.E. Maslen, P.P. Korambath, R.D. Adamson, B. Austin, J. Baker, E.F.C. Byrd, H. Dachsel, R.J. Doerksen, A. Dreuw, B.D. Dunietz, A.D. Dutoi, T.R. Furlani, S.R. Gwaltney, A. Heyden, S. Hirata, C.P. Hsu, G. Kedziora, R.Z. Khalliulin, P.Klunzinger, A.M. Lee, M.S. Lee, W.Z. Liang, I.Lotan, N. Nair, B.Peters, E.I. Proynov, P.A. Pieniazek, Y.M. Rhee, J. Ritchie, E. Rosta, C.D. Sherrill, A.C. Simmonett, J.E. Subotnik, H.L. Woodcock III, W.Zhang, A.T. Bell, A.K. Chakraborty, D.M. Chipman, F.J. Keil, A. Warshel, W.J. Hehre, H.F. Schaefer, J. Kong, A.I. krylov, P.M.W. Gill and M. Head-Gordon, *Phys. Chem. Chem. Phys.*, 8 (2006) 3172.
26. R.G. Parr, R.A. Donnelly, M. Levy, W.E. Palke, *J. Chem. Phys*. 68 (1978) 3801.
27. R.G. Parr, R.G. Pearson, *J. Am. Chem. Soc*. 105 (1983) 7512.
28. I.Lukovits, E. Kalman, F. Zucchi, *Corrosion* (NACE) 57 (2001) 3.
29. M.J.S. Dewar, W. Thiel, *J. Am. Chem. Soc*. 85 (1963) 3533.
30. P.K. chattaraj, U. Sarkar, D.R. Roy, *Chem. Rev*. 106 (2006) 2065.
31. A.Lesar, I. Milosev, *Chem. Phys. Lett*. 483 (2009) 198.
32. B. Gomez, N.V. Likhanova, M.A. Dominguez-Aguilar, R. Martinez-Palou, A. Vela, J.L. Gazquez, *J. Phys. Chem*. B 110 (2006) 8928.
33. R.G. Parr, W. Wang, *J. Am. Chem. Soc*. 106 (1984) 4049.
34. W. Yang, W.J. Mortier, *J. Am. Chem. Soc*. 108 (1986) 5708.
35. N. O. Obi-Egbedi, I.B. Obot, A.O. Eseola, *Arab. J. Chem.* (2010), doi:10.1016/j.arabjc.2010.10.025
36. N. O. Obi-Egbedi, I.B. Obot, A.O. Eseola, *Ind. Eng. Chem. Res*. 50 (2011) 2098.
37. E.E. Ebenso, T. Arslan, F. Kandemirli, N. Caner, I. Love, *Int. J. Quant. Chem*. 110 (2009) 1003.
38. A.Y. Musa, A. H. Kadhum, A.B. Mohamad, A.B. Rohoma, H. Mesmari, *J. Mol. Struct.* 969 (2010) 233.
39. G. Gece, S. Bilgic, *Corros. Sci.* 51 (2009) 1876.
40. I.Ahamad, R. Prasad, M.A. Quraishi, *Corros. Sci.* 52 (2010) 1472.
41. M.K. Awad, M.R. Mustafa, M.M. Abo Elnga, *J. Mol. Struct. (THEOCHEM)* 959 (2010) 66.
42. L. M. Rodrigez-Valdez, A. Martinez-Villfane, D. Glossman-Mitnik, *J. Mol. Struct. (THEOCHEM)* 713 (2005) 65.
43. A.Stoyanova, G. Petkova, S.D. Peyerimhoff, *Chem. Phys*. 279 (2002) 1.
44. R. Hasanov, M. Sadikglu, S. Bilgic, *Appl. Surf. Sci*. 253 (2007) 3913.
45. E.E. Ebenso, D.A. Isabirye, N.O. Eddy, *Int. J. Mol. Sci*. 11 (2010) 2473.
46. M. Sahin, G. Gece, E. Karci, S. Bilgic, *J. Appl. Electrochem*. 38 (2008) 809.
47. S.G. Zhang, W. Lei, M.Z. Xia, F.Y. Wang, *J. Mol. Struct THEOCHEM* 732 (2005) 173.
48. F. Bentiss, M. Lebrini , M. Lagren´ee , M. Traisnel , A. Elfarouk , H. Vezin . *Electrochim. Acta* 52 (2007) 6865.
49. N. O. Eddy , U. J. Ibok , E. E. Ebenso, A. El Nemr, El Sayed, H. El Ashry, *J. Mol. Model.* 15 (2009) 1085.
50. K. F. Khaled, K. Babic-Samradzija, N. Hackerman, *Electrochim. Acta* 50 (2005) 2515.
51. K. F. Khaled, *Appl.Surf. Sci*. 252 (2006) 4120.
52. J.L. Hintze, *NCSS User's Guide*. NCSS, Kaysville, USA. 2006.
53. I.Lukovitis, I. Bako, A. Shaban, E. Kalman, *Electrochim Acta* 43 (1998) 131.

© 2011 by ESG (www.electrochemsci.org)